A new way to measure viscosity in droplet-based microfluidics for high throughput analysis

Estelle André, Nicolas Pannacci, Christine Dalmazzone, Annie Colin

Soft Matter

ARTICLE

A new way to measure viscosity in droplet-based microfluidics for high throughput analysis

Received 00th January 20xx,
Accepted 00th January 20xx

DOI: 10.1039/x0xx00000x

www.rsc.org/

Estelle André [a], Nicolas Pannacci [a], Christine Dalmazzone [a] and Annie Colin [b,c]

In this work, we propose a new way to measure viscosity of samples in a microfluidic device. By analysing the shape of droplets after an expansion, we can measure the viscosity of the phase inside the droplet knowing the surface tension between the two liquids, the flow rate, the geometry of the channel and the viscosity of the continuous phase. This work paves the road for future high throughput studies in the framework of digital microfluidics.

Introduction

Combinatorial chemistry has opened new paths for synthesizing large libraries of novel materials and formulations.[1] High throughput characterization techniques become essential in order to benefit from these new synthesis methods. In fact, a systematic investigation of the relevant properties is required to select the convenient formulation or material. In this paper, we present a setup which allows to perform continuous rheological measurements on a microfluidic chip.

Rheology is the study of the deformation and flow of a material in response to an applied stress. Viscosity is defined as the ratio between the shear stress and the shear rate.[2] For simple liquids, the shear stress is linearly related to the shear rate via the viscosity coefficient. In complex fluids, the existence of a mesoscopic length scale ranging between the molecular size and the whole sample[2] induces coupling between the structure of the fluid and the flow leading to a non-Newtonian behavior. Rheological behaviors are key parameters in many fields, ranging from medicine and food processing to the chemical and manufacturing industries. In the food industry, the stability of dressings is often obtained by increasing the viscosity. In the oil industry, in the field of enhanced oil recovery, the viscosity of the injected polymer solutions has to be higher than that of the oil in order to avoid fingering instability.[3,4] At the opposite, the viscosity of a medication must be low enough to be infused using a needle and a syringe. The development of these products thus requires the use of additives that tune the viscosity of the product to the range required by the final application. The formulation of the appropriate additives in a mixture is a tedious screening work that involves a series of long trials and tests. The use of high throughput microfluidic techniques, in this field would both increase efficiency and reduce costs of research and development for the chemical industry.[5] Let us underline that high throughput tests do not require to measure directly the property under scrutiny i.e. the viscosity of the sample in this study. Their aim is to define the area of a phase diagram where the properties are suited for applications. The measurement of a parameter varying as this property is sufficient to perform these tests. If required the property may be measured afterwards using classical tools.

Measuring rheological properties using high throughput techniques goes through miniaturization of the measurement setup.[6] The easiest type of rheometer to miniaturize, allowing for a continuous approach, are capillary rheometers.[7,8] Galambos and Forster[9] have proposed to use microfluidic devices and to take advantage of the features of specific microfluidics flows. After a T junction, two miscible fluids flowing side by side in the outlet channel are mixed by inter-diffusion. Right after the T junction, the interface between the two fluids is still sharp since in their experimental conditions, diffusion is slower than convection. In the channel, the position of the interface is fixed by the ratio of the flow rates of the two fluids and by the ratio of their viscosities. These authors show that by measuring the position of this interface using fluorescence microscopy, they manage to compute the viscosity of one sample by knowing the flow rates and the viscosity of the other fluid. This elegant method does not require the implementation of an external pressure sensor. It has been improved by Guillot *et al.*[12,13], Lee and Thipathi[14] and Solomon and Vanapalli[15]. The tool is relatively easy to use owing to its simple setup and the absence of direct measurements of pressure.

These techniques are efficient. However, they have to be coupled to a device allowing the preparation of samples of various compositions to be used in a screening approach. One

[a] IFP Energies nouvelles, 1 et 4 avenue de Bois-Préau, 92852 Rueil-Malmaison, France
[b] Paris Sciences Lettres, ESPCI Paris, CBI-,MIE UMR 8321 10 rue Vauquelin 75321 Paris cedex 06 France.
[c] Université de Bordeaux, Centre de recherches Paul Pascal UPR 8641, 115 avenue Schweitzer 33608 Pessac

may inject water and a concentrated solution of polymer at the inlet of a T junction. By varying the ratio of the two flow rates, one obtains, in the outlet channel, mixtures of various compositions. This process requires to flush the fluidic network between two compositions. At least twice the dead volume of the new composition has to be injected to avoid cross contamination of the preparations. Droplet-based microfluidics is more suited than continuous microfluidics for the preparation of samples. It allows the manipulation of droplets or plug of small volumes (10^{-6} to 10^{-15} L) carried and isolated by an immiscible phase. These droplets can be generated at high frequencies (up to 100 kHz), merged with each other, split, trapped, and sorted with hydrodynamic, electrical, and optical-based droplet manipulation techniques.[16-18] In droplet-based systems, since Taylor diffusion and dilution of sample and reagents are absent, the temporal concentration information of samples can be preserved in droplets with high resolution and high fidelity. Such a feature is particularly suitable for high throughput formulations assays.

The main drawback of this approach is the relative absence of characterization techniques.[19] Fluorescent probes or Raman scattering may be used to follow a chemical or biological reaction.

Brosseau *et al.*[20] and Lee *et al.*[21] have extended these characterization techniques to another property than an optical property. Making use of the deformation of a droplet exiting a constriction, they have measured the surface tension and developed an analysis to characterize the features of surfactant adsorption. This type of analysis has also been used before by Cabral *et al.*[22] for the development of a microfluidic tensiometer.

In this work, we extend the previous approach to the measurement of the viscosity of the liquid present inside the droplet. The main originality of our work is to present a viscosimeter for droplet-based microfluidics. The first part of the article is devoted to the description of the materials and of the methods. The second part deals with the experimental results. It is a comprehensive study displaying the variation of the relaxation time and the maximal deformation of a droplet after a constriction as a function of the viscosities of the two phases, the surface tension, the size of the droplet and the velocity of the flow. From this study, we define an experimental protocol (see fourth part) allowing the measurement of the viscosity and apply it to characterize dilute polymer solutions. We show that this analysis may also be used for non-Newtonian fluids. We conclude by giving an example of high throughput experiments. The last part is devoted to conclusion and outlooks.

Materials & methods

Chemicals

The aqueous phase consists of deionized water-glycerol (Sigma-Aldrich) mixtures (60% and 68.4% (w/w), where 0% glycerol is only DI water) and the oil phase is a silicone oil (Polydimethylsiloxane, 20 and 500 mPa.s, Prolabo and VWR) or a mixture of both. Dodecyltrimethylammonium bromide (DTAB, Sigma Aldrich) was used as a surfactant at 1.7% (w/w) in the aqueous phase. This concentration is equal to twice the critical micellar concentration (CMC).

Aqueous polymer solutions were also used. They consist of deionized water-PEG600 (Polyethylene glycol, BioUltra, $\bar{M}_w = 624\ g/mol$, Sigma Aldrich) mixtures (51.9%, 63.3%, 69.9%, 74.6% and 78.3% (w/w), where 0% PEG600 is only DI water).

We used shear thinning and elastic solutions. They consist of HPAM polymer solutions. HPAM are partially Hydrolysed PolyAcrylaMides. They consist of a succession of acrylamide monomers which form a linear chain between them. These polymers are partially hydrolysed and bear an electrical charge. Some of the amide functions are carboxyl or carboxylate functions. The degree of hydrolysis corresponds to the number of hydrolysed units on the total number of units of the polymer. Two solutions of HPAM of different molar masses were studied. The first polymer coined FLOPAAM 3230 has a molar mass of $\bar{M}_w = 9.10^6\ g/mol$ and a degree of hydrolysis of 25 to 30%. The second polymer coined FLOPAAM 3630 has a more important molar mass, $\bar{M}_w = 18.10^6\ g/mol$ and degree of hydrolysis of 25 to 30%. Both are sold by SNF.

The HPAM solutions are prepared in the following manner: the polymer in powder form is solubilized to the desired concentration in deionized water with magnetic stirring overnight at room temperature. In both cases, we worked with dilute solutions (1000 ppm in DI water).

Pendant drop tensiometry

The determination of the interfacial tensions of the aqueous phase-oil phase interfaces is performed using the pendant drop method (Drop Shape Analyser – KRÜSS DSA 25). A glass cuvette is filled with the oil phase. Before each measurement, the cuvette is rinsed with the oil being tested. The syringe and the needle used to produce the droplet are rinsed with the mixture being tested. Drops of aqueous mixtures are formed at the tip of a needle into the oil reservoir. Before each series of measurements, the magnification of the video image is first determined fixing the needle diameter in order to access the drop dimensions. A numerical method based on the Young-Laplace equation is then used to vary a shape parameter known as the Bond number until the calculated drop shape coincides with the actual drop shape. The interfacial tension is calculated from this adapted shape parameter knowing the difference in densities between the two phases.

In the case of the HPAM solutions, the two-phase densities are too close to be measured with the pendant drop method. The corresponding interfacial tensions were therefore measured using the Wilhelmy plate method. A thin platinum plate connected to a microbalance dives into a tank containing one or two liquids if the light phase is not air. The blade is positioned at the interface between the light phase and the heavy phase. The force on the plate due to wetting is

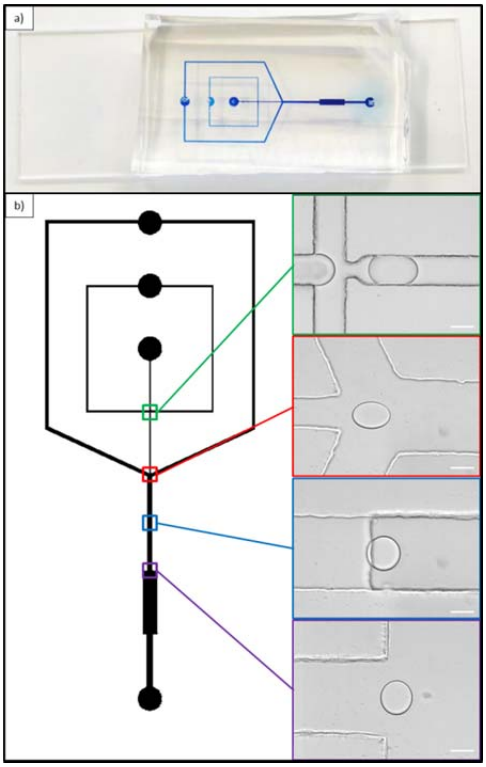

Fig. 1 (a) Picture of the microfluidic chip. (b) Geometry of the microfluidic chip. Droplets are produced at a flow-focusing (green enlarged area) and spaced by a side stream (red enlarged area). The droplets then can be unconfined (blue enlarged area). Then they flow in an expansion (purple enlarged area) where the droplet deformation profile is recorded. The white scale bar has a length of 100 µm.

measured using the microbalance and used to calculate the interfacial tension using the Wilhelmy equation.
All of the results are given with a maximal error of 7%.

Rheology

The determination of the viscosity of the different phases is performed using a Physica MCR-301 (Anton Paar GmbH, Graz, Austria) rheometer. The rheometer was equipped with a temperature controller (C-PTD200-SN928212) and a coaxial cylinder with double air-gap (DG26.7/Q1 – SN36551) or a cone and plate geometry with a diameter of 4 cm and an angle of 1°59 (SN982166).
Measurements are performed at 20°C. The shear rate is varied from 10 to 1000 s^{-1} and data points are taken every 15 s. The value of the viscosity is taken as an average of all the data points obtained over the shear rate range for the Newtonian case. All of the results are given with an error of 5%.

Device design

The microfluidic channel geometries are designed using the layout editor CleWin. These geometries (Fig. 1) consist of a flow focusing junction including the oil phase and aqueous phase inlets. A third inlet is added to control the velocity and the spacing of the droplets. The height of the channels that make up this first part of the geometry is H = 120 µm. A chamber where the deformation of the droplet occurs (Fig. 2) is designed before the outlet of the device. The width of this

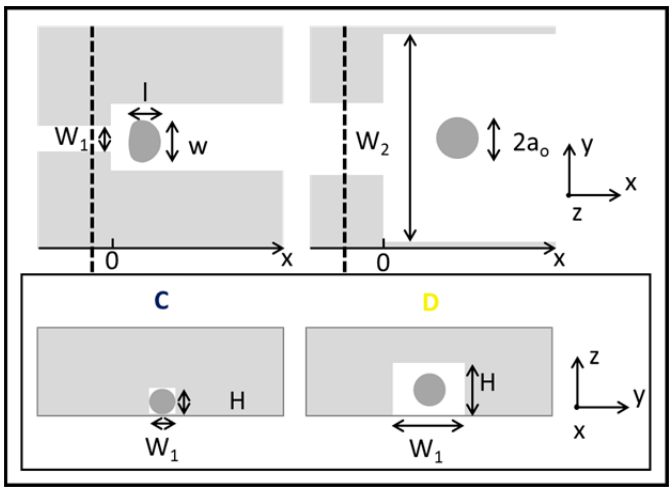

Fig. 2 Diagram of the chamber where the deformation occurs. The upper part depicts the top view of the chamber. In the lower part, the diagram coined "C" refers to the side view of the chamber in the "confined droplet situation" and the diagram coined "D" refers to the side view of the chamber in the "unconfined droplet situation".

chamber is three times greater than the width of the inlet channel. The height of the chamber may differ from the height of the channels that make up the first part of the geometry. Two different geometries were used. The first one refers to the "confined droplet situation" and is coined "C". In this case, the width of the inlet channel is W_1 = 120 µm, the width of the chamber is W_2 = 310 µm and the channel height remains the same all along the chip and equals to H = 120 µm. The second geometry refers to the "unconfined droplet situation" and is coined "D". In this case, the width of the inlet channel is W_1 = 333 µm, the width of the chamber is W_2 = 960 µm and the channel height is equal to H = 120 µm in the first part of the microsystem (Fig. 1 green and red enlarged areas) and to H = 240 µm in the deformation chamber (Fig. 1 purple enlarged area). The droplets flow in this chamber. (Fig. 1 purple enlarged area and Fig. 2). It is the place where their deformation is recorded. In the experiments, the radius of the droplets is varied between 20 µm to 85 µm. The velocity of the droplets range between 10 mm/s to 260 mm/s.
In the following, we will define a geometrical parameter as $R^*=2a_o/W_1$ where a_o is the radius of the droplet, W_1 the width of the inlet channel at the entrance of the chamber.
Brosseau *et al.*[20] use the same geometrical parameter in their analysis.

Microfabrication

Microfluidic devices are produced using standard photolithography techniques using photomasks (Photext). In brief, a negative mold of the structure is prepared by photolithography of SU8-2100 (Micro Chem) on a silicon wafer. Polydimethylsiloxane (PDMS, RTV 615, Momentive) was poured over the mold, cured in an oven for at least 2h at 65°C and peeled off the mold. The holes for the tubing connections are punched with a biopsy needle. To seal the device, glass-PDMS or PDMS-PDMS surfaces were oxidized using air plasma. The resulting device can either be treated with a solution of octadecyltrichlorosilane (OTS) in hexadecane to render the

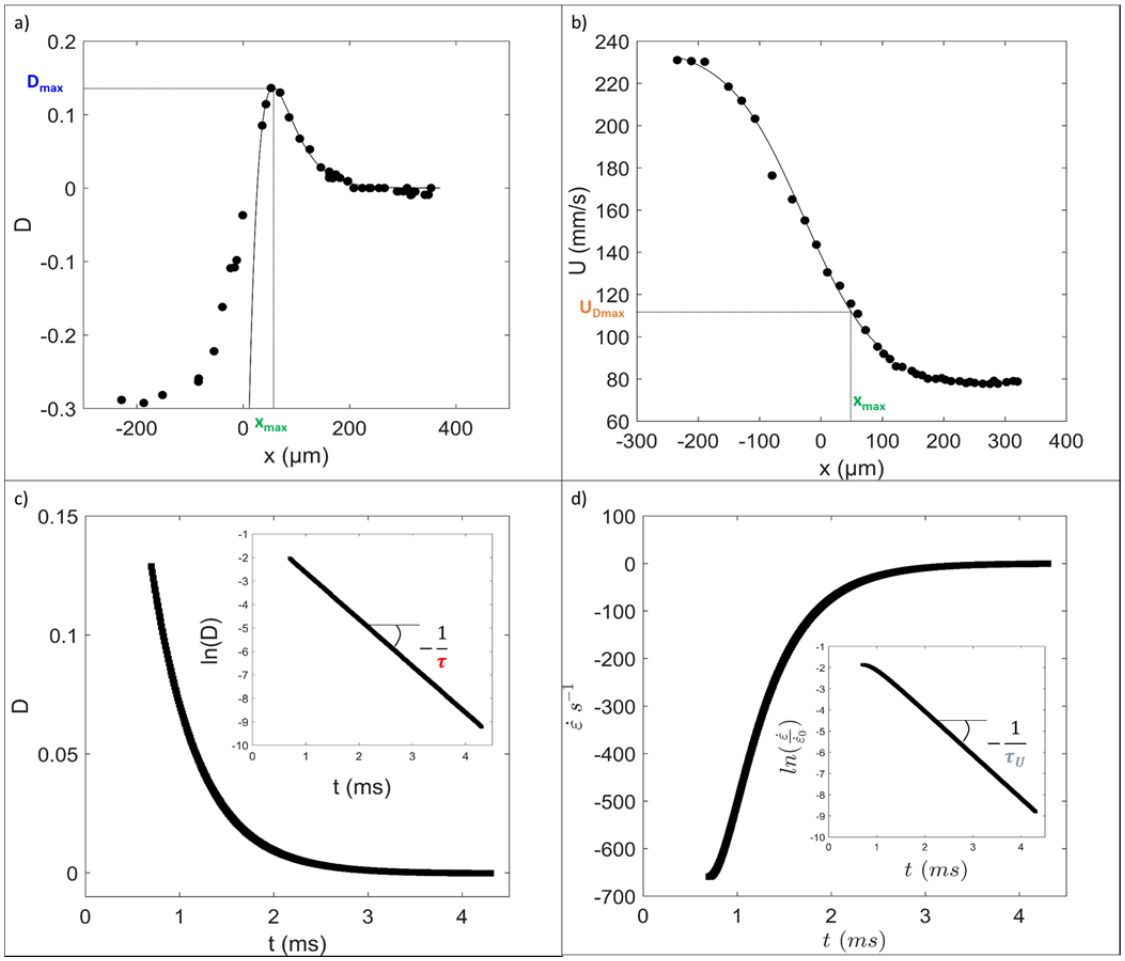

Fig. 3 (a) Typical deformation profile of a droplet passing through the expansion. We can follow the evolution of the deformation as the droplet is in the entrance channel, enters the expansion and relaxes to a spheroid shape. The maximal deformation of the droplet is extracted from this curve. (b) Typical velocity profile of a droplet passing through an expansion. The droplet speed at the maximal deformation is extracted from this curve. (c) Typical deformation profile of a droplet as a function of time. The insert depicts the logarithm of the deformation as a function of time, this graph is used to determine the relaxation time of the droplet. (d) Typical profile of the extension rate as a function of time. The insert depicts the logarithm of the normalized extension rate as a function of time, this graph is used to determine the convection time of the droplet. (For this figure, fluids are a silicone oil 20 cSt for the droplet phase and a DI water-glycerol mixture 60% (w/w) for the continuous phase. The radius of the droplet is 76 μm and we use set up C. The surface tension is 28 mN/m, the initial velocity of the droplet is 246 mm/s).

channel walls hydrophobic[23] or poly(acrylic acid) can be grafted on the channel walls to render them hydrophilic[24]. In order to vary the height of the device between the channel and the chamber, two patterned PDMS surfaces can be sealed by adding EtOH between the two surfaces just after the plasma treatment. The two surfaces can thus be aligned manually in a timescale of 30 min. The aligned surfaces are then placed in an oven overnight. The channel height was measured by image analysis cutting the channel after experimentation.

Microfluidics

The fluids are injected from reservoirs using a pressure driven flow controller (Fluigent MFCS EZ). Reservoirs and the microfluidic chip are connected via PEEK (PolyEtherEtherKetone) tubing of outer diameter 500 μm or FEP (Fluorinated Ethylene Propylene) tubing of outer diameter 1/16''.

High-speed microscopy

The microfluidic device is mounted on an inverted microscope (Axio Observer Mat, Zeiss) and imaged using a x20 microscope objective. The pictures of the droplets are recorded with a high-speed camera (i-SPEED 2, Olympus) at a frame rate of 2000 or 4000 pictures per second. The movies of droplets are recorded at the entrance of the deformation chamber.

Image processing and data analysis

The droplet trajectory and shape are obtained by image processing of the high-speed movies through plug im !25 an open software platform for data processing from IFPEN already used for other case studies[26].

All parameters of interest rely on the detection of the two-dimensional projection of the contour of the droplet. The droplet contour is defined as the outside edge of the droplet meniscus. Different parameters are extracted from this analysis: the droplet width *w*, the droplet length *l* and the droplet centre positions *x*, *y* (Fig. 2). Then a home-made Matlab program is used to obtain the parameters of interest. Fig. 3 displays typical results.

For each droplet, the deformation *D* is defined as:

$$D = \frac{w-l}{w+l} \quad (1)$$

and is obtained as a function of the position in the channel (Fig. 3 (a)). For each measurement, the values obtained for 3 droplets are considered. The uncertainty on the measurement is $\Delta D = 0.003$.

Following Gires *et al.*[27], the maximal deformation in the expansion D_{max} is obtained by a fitting of the deformation curve with the following equation:

$$D = p_1 + (p_2 + p_3 x) exp(-x/p_4) \quad (2)$$

p_i are the fitting parameters.
This fitting is performed only on the data for those where the droplet is in the expansion chamber. The position x_{max} corresponding to the maximal deformation is also extracted.
The droplet instantaneous velocity is defined as:

$$U = \frac{x(i+1)-x(i)}{t_f} \quad (3)$$

i.e. the division of the difference in position of the center between two frames *i* and *i+1* by the time between two frames t_f. The droplet velocity is then plotted as a function of its position in the channel (Fig. 3 (b)) and the resulting curve is fitted with the following equation:

$$U = p_1 + p_2 tanh\big(p_3(x + p_4)\big) \quad (4)$$

The speed of the droplet at the maximal deformation U_{Dmax} is extracted from this fitting. Then combining fitted data of deformation and velocity, the deformation of the droplet is obtained as a function of time. The relaxation time of the droplet τ is obtained by a linear fitting of the curve representing the logarithm of the deformation as a function of time (Fig. 3 (c)). For the following, we define $\dot{\varepsilon} = dU/dx$ as the extension rate of the droplet and plot it as a function of time (Fig. 3 (d)). We also define a convection time obtained by a linear fitting of the curve representing the logarithm of the normalized extension rate as a function of time (Fig. 3 (d) Insert).

Experimental results

We first focus on simple systems and study the deformation of droplets made of silicone oil. The continuous phase is a water-glycerol mixture. In some situations, dodecyltrimethylammonium bromide (DTAB) is used as a surfactant. It is dissolved in the aqueous phase. In the following, we discuss first the measurement of the relaxation time.

Relaxation time

Fig. 4 gathers all the experiments performed. In those experiments, the radius of the droplet a_o is typically comprised between 40 and 85 µm, the height of the chamber *H* between 120 and 240 µm, the geometrical parameter $R^* = 2a_o/W_1$ between 0.4 and 1.3, the velocity of the droplet at the maximal deformation U_{Dmax} between 10 and 260 mm/s and the interfacial tension γ between 9.3 and 28 mN/m.
The viscosity of the internal phase η_{int} varies between 20 and 100 mPa.s, the one of the external phase η_{ext} between 10 and 20 mPa.s and the ratio of viscosity between the two phases $\lambda = \eta_{int}/\eta_{ext}$ between 1 and 10.

All the data collapse on a master curve. The relaxation time is given by:

$$\tau = \frac{3}{4}\frac{W_1}{U_{Dmax}} \quad (5)$$

Strikingly, the characteristic time involved in the relaxation of the shape of the droplet does not depend upon the interfacial tension. We have checked this point experimentally by comparing measurements performed in presence and in absence of surfactants. In our experiments, we used DTAB at a concentration of 0.07 mol/L which is above the CMC (CMC = 0.03 mol/L[36]). Let us anticipate that in this situation the interface of the drops was always covered by surfactants (see next section).
The radius of the droplets in presence of surfactant is 76 µm, the velocity 125 mm/s, the viscosity of the dispersed phase 19 mPa.s, the viscosity of the continuous phase 11.8 mPa.s, the relaxation time is 1.6 ms). In this situation, the surface tension was 9.3 mN/m.
In absence of surfactant, the radius of the droplets in presence of surfactant is 78 µm, the velocity 136 mm/s, the viscosity of the dispersed phase 19 mPa.s, the viscosity of the continuous phase 11.8 mPa.s, the relaxation time is 1.6 ms. The surface tension is equal to 27.7 mN/m.

Deformation

Fig. 5 and Fig. 6 display the measurements of the maximal deformation as a function of the combination of the capillary number, the geometrical parameter and the ratio of viscosity. The capillary number is defined as:

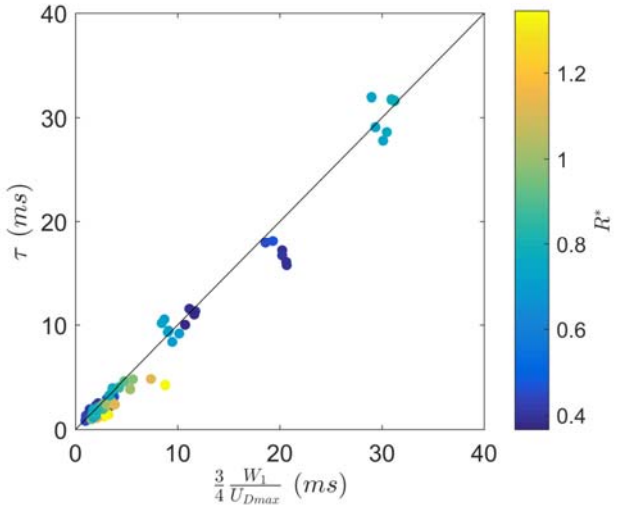

Fig. 4 Collapse of the droplet relaxation time on a master curve. Data are from all the experiments performed in the confined and the unconfined droplet situation. The colorbar specifies the value of the geometrical parameter R*.

$$Ca = \frac{\eta_{ext} U_{Dmax}}{\gamma} \quad (6)$$

γ is the interfacial tension.

This number varies between 0.01 and 0.12 in these experiments. We have not been able to collapse all the data on a single curve independent of the confining regime.

The data have been separated on two graphs. Fig. 5 deals with confined droplets ($R^* > 0.7$) whereas Fig. 6 focuses on unconfined droplets ($R^* < 0.7$). We split our analysis at $R^* = 0.7$. This may seem striking. The change of behavior does not always occur for critical parameters equal to 1. For example, turbulence occurs for Reynolds number much higher than 1. Here we think that the presence of a lubrication film between the wall of the channel and the droplet induce a change of behavior for *R** less than 1.

When the droplet is confined in the channel, a lubrication film is formed between the channel wall and the droplet. The majority of the studies concerning the calculation of the thickness of this film in the case of two-phase flows concern gas-liquid systems. Since Bretherton[28] which provided an estimate of the lubrication film thickness for very low capillary numbers in circular-section channels, the models have extended to wider ranges of capillary numbers and to square channels. Whatever the model considered and the conditions, the thickness of this film increases with a power of the capillary number $Ca^{\alpha}$with $\alpha > 0$.

Thus, the lower the interfacial tension or the higher the viscosity of the continuous phase, the thicker the film. The presence of this film can create additional dissipation forces that will hinder the deformation of the droplet. Thus, the larger the capillary number, the more the droplet is hindered in its deformation and the more the exponent associated with the capillary deviates from 1 by decreasing.

Knowing this, it is still mathematically possible to look for a scaling law (Fig. 5). The maximal deformation scales as:

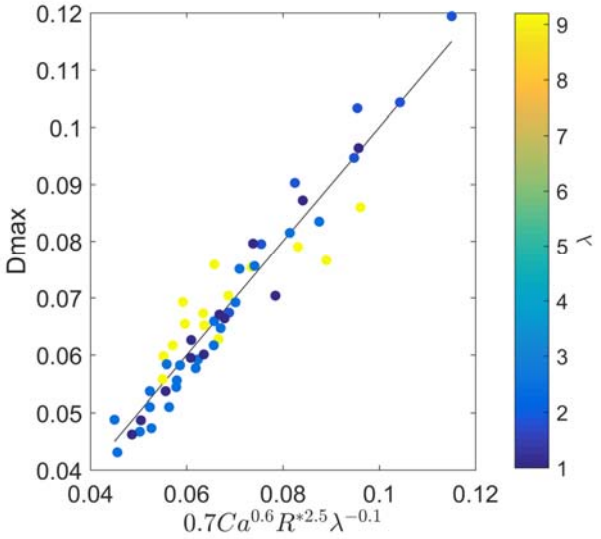

Fig. 5 Collapse of the droplet maximal deformation on a master curve $D_{max} = 0.7Ca^{0.6}R^{*2.5}\lambda^{-0.1}$ in the confined droplet situation. The colorbar specifies the value of the viscosity ratio λ.

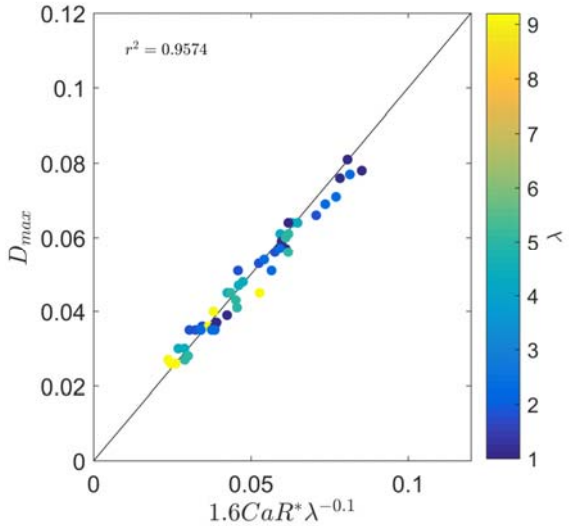

Fig. 6 Collapse of the droplet maximal deformation on a master curve $D_{max} = 1.6CaR^*\lambda^{-0.1}$ in the unconfined droplet situation. The colorbar specifies the value of the viscosity ratio λ.

$$D_{max} = 0.7Ca^{0.6}R^{*2.5}\lambda^{-0.1} \quad (7)$$

This function has been determined by fitting the experimental data with a mean squared procedure. The coefficient of determination here is r^2 = 0.92. This value is mainly due to the fact that, as we explained previously, it is not possible to find a general scaling law valid for all viscosities and interfacial tensions as the exponents vary with these properties.

This conclusion differs in the unconfined droplet situation (Fig. 6). The maximal deformation scales as:

$$D_{max} = 1.6CaR^*\lambda^{-0.1} \quad (8)$$

The coefficient of determination is higher and equal to 0.96. The exponent of λ is equal to -0.1. This slight dependence allows the measurement of the viscosity of the internal phase.

Analysis of the data

Let us now discuss the obtained results. At the end of this section, we will define an experimental procedure to measure the viscosity of the sample located inside the droplet.

We have first shown that the relaxation time does not depend upon the interfacial tension. To understand this point it is required to analyze the relaxation of a droplet submitted to a flow. The modelling of this process has been first addressed by Taylor[29]. In Taylor's model a droplet of viscosity η_{int} is placed in a fluid with a viscosity η_{ext}. The system is submitted to a pure hyperbolic flow in the (x,y) plane. In this situation, the extension rate along the flow direction x , $\dot{\varepsilon} = \mathrm{dU}/dx$ is a constant. *U* is the velocity of the surrounding fluid. The steady deformation (i.e. the deformation of the drop when steady state is achieved) is proportional to the extension rate and is given by:

$$D_{steady} = \frac{19\lambda+16}{16\lambda+16}\left(\frac{2\eta_{ext}\, a_0}{\gamma}\right)\dot{\varepsilon} \quad (9)$$

γ is the interfacial tension, D_{steady} is the steady deformation of the droplet i.e after the relaxation process.

Note that a sharp constriction induces an inhomogeneous extensional velocity field. The use of a geometry involving a uniform extensional flow rate would allow us to use this formulation and to measure the viscosity through the measurement of D_{steady} knowing the interfacial tension. Even though some optimized geometries have been proposed by Zografos *et al.*[30], they remain devoted to one phase flow and induce a homogeneous elongational rate only in the middle plane of the channel. As they are complex to set up experimentally, we decided to use a sharp constriction.

As we just mentioned, a sharp constriction induces an inhomogeneous extensional velocity field. This theoretical model has been generalized to inhomogeneous extensional velocity fields by Barthes-Biesel *et al.*[31] and summarized by Rallison[32] and Trégouët *et al.*[33].

Following this last work, the steady deformation must be calculated with the mean values of the eigenvalues <e1> and <e2> of the deformation-rate tensor averaged over the drop through:

$$D_{steady}(\mathrm{t}) = \frac{19\lambda+16}{16\lambda+16}\left(\frac{2\eta_{ext}\, a_0}{\gamma}\right)(< e_1(t) > - < e_2(t) >) \quad (10)$$

Barthes-Biesel *et al.*[31] assume that the transient regime is captured by a first-order relaxation towards the steady state D_{steady}:

$$\frac{dD}{dt} = \frac{1}{\tau_{ca}}(D_{steady}(\mathrm{t}) - D) \quad (11)$$

where:

$$\tau_{Ca} = \frac{2}{5}(2\lambda+3)\frac{19\lambda+16}{16\lambda+16}\frac{a_o\eta_{ext}}{\gamma} \quad (12)$$

Note that the capillary time does not depend upon the velocity.

To solve this set of equations, numerical simulations are required to compute the eigenvalues $<e_1>$ and $<e_2>$. These numerical simulations are out the scope of this work. To go further, we proceed through hypothesis and restrict our analysis to our experimental situation. We assume that D_{steady} varies exponentially with the distance to the inlet of the chamber. This point is in agreement with the recent numerical simulations of Trégouët *et al.*[33]

The correspondence between time and space in microfluidic devices allows us to write:

$$D_{steady}(\mathrm{t}) = D_o exp^{(-Ut/L)} \quad (13)$$

where *U* is the velocity of the droplet, *L* a characteristic length, D_o the initial value of the deformation and t the time.

We define a convection time $\tau_U = L/U$.

Note that we assume here that the velocity of the dispersed phase is proportional to the velocity of the droplet. The dynamics of droplets in microfluidic devices has been extensively studied by Gallaire and co-workers. In a review[34], they show that the velocity of a drop differs slightly from the velocity of the fluid in rectangular geometry. In this situation, the flow in the gutters of the geometry governs the differences of velocity. The ratio $(U - V_d)/U$ scales as $B\, Ca^{-1/3}$ where *B* is a constant. *U* is the velocity of the drop and V_d the mean velocity of the dispersed phase. In all the cases, the differences between *U* and V_d are less than 6%. In our analysis, we neglect this non-linear variation and assume that the velocity of the drop U is proportional to the mean velocity of the fluid V_d.

The solving of this set of equations shows that:

$$D(t) = C_1 exp^{-t/\tau_{Ca}} + C_2 exp^{-t/\tau_U} \quad (14)$$

where C_1 and C_2 are two constants and also shows that:

$$D(t) \approx D_{steady}(t) \quad (15)$$

for $t \gg \tau_{Ca}$ and $\tau_U \gg \tau_{Ca}$.

Our experiments follow this hypothesis since the time scale involved in the relaxation process is 2.5 to 32 times higher than the time calculated for the capillary relaxation.

Experimental data displayed on Fig. 4 suggest that our experiments follow the framework of the previous analysis. They show that the relaxation of the droplet involves a single time scale inversely proportional to the velocity. The characteristic length *L* involved in the spatial development of the flow is proportional to W_1 the width of the inlet channel at the entrance of the deformation chamber.

This analysis is confirmed quantitatively by the fact that the time scale involved in the extensional velocity field is the same than the relaxation time of the deformation. In Fig 3, the relaxation time involved in the extensional flow is 0.5 ms. 0.5 ms is also the relaxation time of the deformation in this situation while the corresponding capillary time is equal to 0.08 ms.

These results clearly show that in our experiments, the relaxation time cannot be used to measure interfacial tension or viscosity since it is ruled by convection processes. We have tried to vary the size of the channel, of the droplets, to accelerate the flow but we did not succeed to obtain a range of parameter where the convection time τ_U is shorter than the capillary one τ_{Ca}. τ_{Ca} might be measured in the first part of the deformation of the drop around D_{max} i.e. in the short time situation. This measurement is tricky and requires the knowledge of the viscosity of the liquid trapped in the drop to calculate the eigen values of the strain rate tensor and determine precisely D_{steady}.

This analysis points out that the only way to fit the entire curve of relaxation is to use numerical simulations. The extraction of the interfacial tension and viscosity of the internal phase require to assume values, fit the data and make back and forth between experiments and numerical simulations. This procedure has been used recently by Trégouët *et al.*[33] to measure the interfacial tension.

In this work we chose an experimental approach and decide to use a calibration curve. We determine the value of the maximal deformation D_{max} experimentally. We assume that this value is a function of the physical quantities that control the problem i.e. the droplet velocity and radius, the interfacial tension and the viscosity of the two fluids. Looking for a scaling law, we expect that the capillary number, the geometrical parameter and the ratio of viscosity are involved in this relationship linking the maximal deformation to the previous dimensionless numbers.

Brosseau *et al.*[20] found a relationship involving the capillary number and the geometrical parameter only, keeping the ratio of viscosity constant. However, Park and Dimitrakopoulos showed through simulations that this number has an influence on the deformation of the droplet.[35]
In our experiments, we varied this ratio of viscosity to complete the relationship between the maximal deformation and the dimensionless numbers controlling the phenomenon.

Measurements of the maximal deformation evidence two regimes.
We recall that in the confined droplet situation (i.e. for $R^* > 0.7$), the maximal deformation scales as $D_{max} = 0.7Ca^{0.6}R^{*2.5}\lambda^{-0.1}$. But the exponents vary with the properties of the fluids. In the unconfined droplet situation (i.e. for $R^* < 0.7$), the maximal deformation scales as $D_{max} = 1.6CaR^*\lambda^{-0.1}$. The exponent of λ is equal to -0.1. Note that the exponent of *Ca* has been set to one in this analysis as we expect linear effects involving the velocity.

From this law, we propose a procedure to measure the internal viscosity of a droplet. We will first measure the interfacial tension at equilibrium of the droplet. We will assume that this parameter does not vary too much due to elongation. In other words, we will assume that the elasticity of the monolayer is negligible and that no surface gradients are involved during the relaxation. This hypothesis is in agreement with previous studies performed with solutions of surfactants above the critical micellar concentration (CMC) in microfluidic systems.[36] It is also supported by our experimental data. In our experiments, we used DTAB at a concentration of 0.07 mol/L which is above the CMC (CMC = 0.03 mol/L[36]). The measurements performed in presence and in absence of surfactant collapse on the same master curve on Fig. 6.
Note that we have checked following Wang *et al.*[37] and Moiré *et al.*[36] that in this situation the interface of the drops was always covered by surfactants.
The kinetics of adsorption in microfluidic devices has been studied carefully by Wang *et al.*[37] and Alvarez *et al.*[38]. DTAB are small molecules and it is it is demonstrated in the literature that the limiting step is not the adsorption but rather the convection diffusion process. Following Wang and Alvarez, the time scale involved in the diffusive process is $\tau_m = min(h_p, h_c)^2/D_{eff}$ where h_p is the mass transfer distance in a stationary flow and h_c the mass transfer distance in presence of flow. h_p is given by $h_p = \Gamma/C$, where Γ is the surface concentration and C the surfactant monomer bulk concentration. Following the data of Wang and assuming a rigid interface, h_c is given by $h_c = a_o\,(2\pi/(3Pe))^{1/2}$ where a_o is the radius of the droplet or of the jet and *Pe* is the Péclet number defined as $Pe = a_oU/(2D_{eff})$. *U* is the characteristic velocity in the external phase and D_{eff} is the effective diffusion coefficient that takes into account the contribution of the micelles to the mass transfer**.** Following Glawdel and Ren[39], $D_{eff} = D(1+b)(1+bNa^{-2/3})$ where $b = (C/CMC) - 1$, *c* is the surfactant concentration, *CMC* is the micellar concentration and Na is the aggregation number of micelles.
In our situation, Γ_{DTAB} = 1.89 10^{-6} mol/m^2, D_{eff} = 4 10^{-11} m^2/s.[36]
The mass transfer distance in stationary flow h_p is equal to 0.062 mm. The mass transfer distance under flow h_c varies between 1 and 3 mm in our experiments.
The diffusion time is thus equal to 10^{-4} s which is much less than the time scale involved in our experiments (a few milliseconds in our experiments). We may thus consider that the surfaces are saturated by surfactant after the formation and during the expansion of the droplet.
This situation differs from the one presented by Brosseau et al.[20] The surfactant used by Brosseau *et al.* is very specific with a high molecular weight. For these reasons the authors are able follow the kinetics of adsorption in microfluidic device. Note that this situation is not the generic one. For surfactants with moderate molecular weight, the adsorption of the surfactant at the interface is almost instantaneous in microfluidic device as shown by Wang and Moiré.
We anticipate that our method will be not valid in presence of surfactant if the time scale of adsorption or of diffusion is longer than a few ms.

To continue with the procedure, we will measure the velocity of the droplets, its maximal deformation and compute its viscosity.
We underline that our procedure holds for both Newtonian and non-Newtonian systems. We will comment this point in the following section in which we display such a study.

A new method to measure the viscosity in droplets

a/The Newtonian situation

We prepared solutions of PEG at various concentrations. We measured the rheological properties of these solutions using classical rheometry tools. The solutions are Newtonian in the range of studied shear rate. We then used the microfluidic device D and studied the deformation of droplets containing these solutions. We measured the velocity of the droplets and their deformation in the chamber as previously described.
Fig. 7 displays the measurement of the viscosity extracted from the microfluidic analysis as a function of the viscosity measured using a rheometer. The value extracted from the microfluidic analysis is clearly proportional to the one measured using a rheometer. The discrepancy between both is

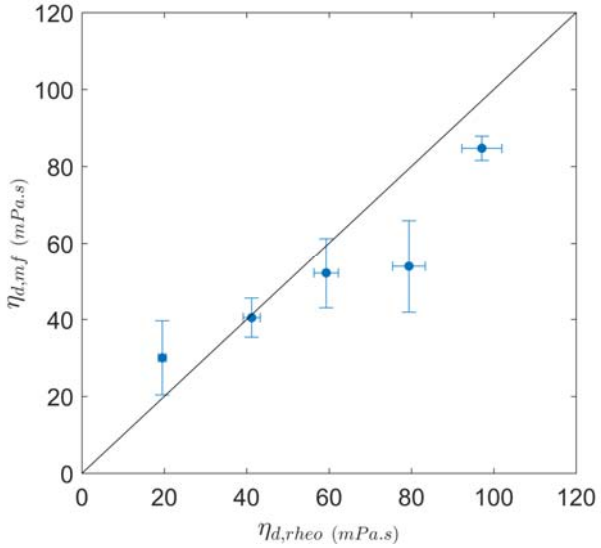

Fig. 7 Measurement of the viscosity extracted from the microfluidic analysis as a function of the viscosity measured using a rheometer of PEG solutions at various concentrations (51.9%, 63.3%, 69.9%, 74.6% and 78.3% (w/w)).

mainly due to the low value of the exponent of λ, that induces a large error bar. These data prove that this method is performant to study the relative evolution of the viscosity of a solution as a function of the concentration of a viscosity enhancing agent. In the framework of high throughput analysis, such correlation is sufficient to find a functioning point for a formulation. If required, the viscosity of the most efficient sample may be measured using a classical rheometer afterwards.

b/The non-Newtonian situation

Tests were carried out in microsystem D with silicone oil as the continuous phase and aqueous solutions of FLOPAAM 3630 and 3230 at 1000 ppm as the dispersed phase. The silicon oil is a Newtonian fluid and its viscosity is 20 mPa.s. Both FLOPAAM solutions are shear thinning solutions. Their rheological curves have been measured in cone plate geometry. These fluids follow a power law equation. Their viscosity is given by $\eta = A\dot{\gamma}^n$ in the measured shear rate range (i.e between 10 s^{-1} and 1000 s^{-1}). We get A = 0.64 and n = -0.71 in the FLOPAAM 3630 situation and A = 0.52 and n = -0.64 in the FLOPAAM 3230 situation. FLOPAMM 3230 solution does not exhibit measurable first normal stress difference. At the opposite, for shear rate higher than 50 s^{-1}, first normal stress differences are of the order of the shear stresses in the FLOPAAM 3630 situation. This last solution is thus shear thinning but also highly elastic.

We used the previous approach to measure the rheological curve for these two solutions. We prepared droplets of polymer solutions. The mechanism of drop formation depends upon the elasticity of the solution.

When a droplet is produced in a continuous phase, a jet of liquid connecting the arrival of dispersed phase to the droplet before its complete detachment is formed. In the Newtonian situation, the diameter of the filament decreases exponentially (regime dominated by the inertia of the continuous phase), then linearly until rupture of the filament to form the droplet (regime dominated by capillary forces).

In the elastic case, an intermediate regime is observed during which the state of the filament results from the equilibrium between elastic forces and capillary forces: the capillary pressure tends to thin the filament, while the elastic forces induced by the stretching fluid resist this thinning. The filament radius also decreases exponentially over time but more slowly. In addition, before its complete breakup, the filament adopts a particular structure consisting of a string of spherical drops connected by fluid bridges called beads-on-a-string. After the complete stall of the droplet, the small drops move very quickly in the centre of the channel, coalesce and integrate with the droplet that has just unhooked. Thus, we are not bothered by the presence of satellite drops during the subsequent analysis of the deformation of the droplet.

For each test involving one of the two polymers, the speed of the drop is varied between 130 and 170 mm/s in the FLOPAAM 3230 situation and between 90 and 140 mm/s in the FLOPAAM 3630 situation. The drop radius is 63 μm ± 5% for the FLOPAAM 3230 and 70 μm ± 3% for the FLOPAAM 3630. The deformation of the drop, its speed and its size are measured in the same way as for the Newtonian fluids. Then, using the correlation found for Newtonian fluids, the corresponding viscosity ratio is determined by:

$$\lambda_N = \left(\frac{D_{max}}{1.6} R^* Ca\right)^{-0.1} \quad (16)$$

Sarrazin *et al.*[40] showed that the velocity profile in the droplet follows a parabolic shape similar to the profile of the Poiseuille flow in which it flows. A droplet positioned near the centre of a Poiseuille flow undergoes internal recirculation. The fluid flows to the front of the drop near its centre and to the back near the interface. Hudson *et al.*[41] used the method presented by Nadim and Stone[42] to determine the flow field inside a droplet created by a Poiseuille flow in a rectangular channel. The expressions characterizing the flow field in the droplet are valid only for unconfined droplets which do not feel the presence of the walls of the channel.

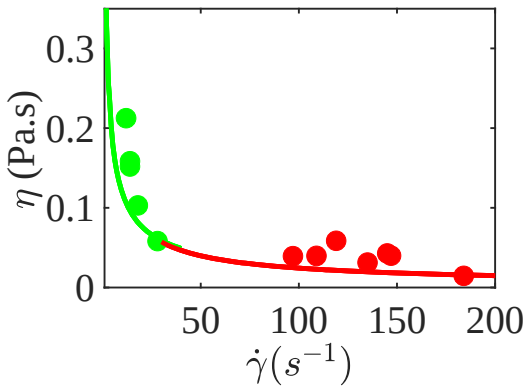

Fig. 8: Droplets viscosities measured by the microfluidic approach as function of the calculated mean shear rate into the droplets. Fluids are FLOPAAM 3230 (green dots) and 3630 (red dots) at 1000 ppm. The dots are measured using our set up and the lines are the viscosity from the rheometer.

For Newtonian fluids, the mean shear rate borne by a drop in an unconfined geometry is given by:

$$\dot{\gamma}_{moy} = \frac{9}{4a_0} \frac{\left(\frac{2a_0}{H}\right)^2}{2(1+\lambda_N)\left(1-\left(\frac{2a_0}{H}\right)^2 \frac{\lambda_N}{2+3\lambda_N}\right)} U_{Dmax} \quad (17)$$

In the following, we will assume that this equation is also valid in the non-Newtonian situation. This may be surprising. We underline that such approach is used classically in all the rheometers.

Fig. 8 displays the obtained results. We note a good agreement between the measured viscosity into the drops and the one measured using a conventional rheometer. We anticipate that in some situation the discrepancy is higher than 40%. However, such measurements are enough accurate in a high throughput approach.

Towards high throughput measurements

In order to show that our technics is promising for high throughput measurements, we developed a microdevice allowing us to measure the viscosity of a mixture as a function of the concentration of its constituents. The geometry we have chosen is shown in Fig. 9. The geometry is similar to the previous ones, but instead of a single arrival of dispersed phase, the geometry has two, one for each of the two solutions involved in the mixture. We inject into the microsystem two aqueous solutions of glycerol at different concentrations. Solution A is composed of 64 % (w/w) of glycerol and solution B with 89 % (w/w) of glycerol. These two solutions are injected at different flow rate ratios using syringe pumps to obtain different dispersed phase viscosities. In order to get a homogenous solution before preparing the droplets, it is required to mix the two fluids. This process is very complex in microfluidics. Two fluids that are injected into a microchannel flow side by side and are only mixed by diffusion.

The characteristic time for diffusion is given by $t_{diff} = W^2/4D_{diff}$ where W is the width of the channel and D_{diff} the diffusion coefficient. A microfluidic channel with a length of $V * t_{diff}$ is thus required to ensure mixing by diffusion, V being the fluid velocity. For an average speed of 5 mm/s and a diffusion coefficient D_{diff} equal to 5.10^{-11} m^2/s, we obtain a length of 1 m, which can not be realized in a fluidic circuit. In order to solve this issue, we use a passive mixer with herringbones that break the flow laminarity and promote mixing between two fluids by increasing the contact surface. This set up is classically used in microfluidic devices. We chose the same herringbones cycles than those of Stroock[43]. They are composed of twice six herringbones. These herringbones are asymmetric, the angle they make with the x-axis of the channel is 45° and the ratio between the shortest and the longest side is of 1:2. In addition, the herringbones are drawn in positive at the top of the channel for better mixing performance.[44] Following the analysis of Stroock, we use 9 cycles of 12 herringbones to ensure the mixing.

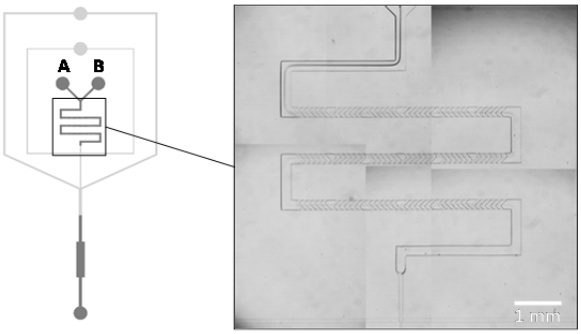

Fig. 9: Geometry of the high-throughput microsystem. The geometry is similar to the previous one but there are two inlets of dispersed phase A and B and a mixing zone.

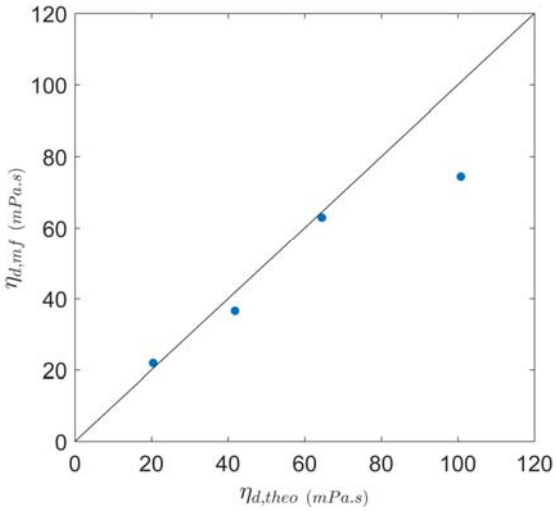

Fig. 10 Measurement of the viscosity extracted from the microfluidic analysis as a function of the viscosity measured using a rheometer of glycerol mixtures at various concentrations (69.2 %, 76.9 %, 80.6 % and 84.2 % (w/w)).

After this mixing zone, the solution enters the droplet formation zone. Droplets are produced and send into an expansion chamber. We measure the viscosity using our approach and the scaling law obtained previously. Fig. 10 shows the viscosity value as a function of the theoretical viscosity given by the flow rate ratios. A good match of these two values is found.

The results presented in this section provide a first step towards a high-throughput analysis of the viscosity of microfluidic droplets. Indeed, thanks to the mixer, we have shown that it is possible to put in contact two different compounds and to mix them to then have access to the viscosity of the resulting mixture.

Conclusion

In this work we have analyzed the flow of droplets inside an expansion. Following the work of Brosseau *et al.*[20], we have shown that the maximal deformation in the unconfined situation depends upon the capillary number, a geometrical parameter and on the viscosity ratio between the internal phase and the external one.

We have thus proposed to use an experimental scaling law to describe the evolution of the maximal deformation D_{max} as a function of the capillary number, the geometrical number and the ratio of viscosity.

We have shown that this analysis was relevant and allowed us to measure the relative evolution of the viscosity of Newtonian and non-Newtonian polymer solutions. This paves the road for high throughput analysis in the framework of digital microfluidics.

Conflicts of interest

There are no conflicts to declare.

Acknowledgements

We thank S. Perrin, C. Burnichon, B. Betro and N. Palazzo for their experimental advices and M. Moreau for the software platform plug im !.

Notes and references

1 P. S. Dittrich and A. Manz, *Nat. Rev. Drug Discovery*, 2006, **5**, 210-218.
2 R. G. Larson, The structure and rheology of complex fluids (Vol. 150), Oxford university press, New York, 1999.
3 G. M. Homsy, *Annu. Rev. Fluid Mech.*, 1987, **19**, 271-311.
4 R. Lenormand, E. Touboul and C. Zarcone, *J. Fluid Mech.*, 1988, **189**, 165-187.
5 A. Colin, T. M. Squires and L. Bocquet, *Soft Matter*, 2012, **8**, 10527-10529.
6 A. Dhinojwala and S. Granick, *The Journal of chemical physics*, 1997, **107**, 8664-8667.
7 C. Clasen and G. H. McKinley, *J. Non-Newtonian Fluid Mech.*, 2004, **124**, 1-10.
8 P. Abgrall and N. T. Nguyen, *Anal. Chem.*, 2008, **80**, 2326-2341.
9 P. Galambos and F. Forster, ASME Int. Mech. Eng. Cong. Exp., Anaheim, CA, 1998, 187-191.
10 K. Kang, L. J. Lee and K. W. Koelling, *Exp. Fluids*, 2005, **38**, 222-232.
11 J. Chevallier and F. Ayela, *Rev. Sci. Instrum.*, 2008, **79**, 076102.
12 P. Guillot and A. Colin, *Microfluid. Nanofluid*., 2014, **17**, 605-611.
13 P. Guillot, T. Moulin, R. Kotitz, M. Guirardel, A. Dodge, M. Joanicot, A. Colin, C-H. Bruneau and T. Colin., *Microfluid. Nanofluid.*, 2008, **5**, 619-630.
14 J. Lee and A. Tripathi, *Anal. Chem*., 2005, **77**, 7137-7147.
15 D. Solomon and S. A. Vanapelli, *Microfluid. Nanofluid.*, 2014, **16**, 677-690.
16 S. Y. Teh, R. Lin, L. H. Hung and A. P. Lee, *Lab Chip*, 2008, **8**, 198-220.
17 N. Lorber, F. Sarrazin, P. Guillot, P. Panizza, A. Colin, B. Pavageau, C. Hany, P. Maestro, S. Marre, T. Declos, C. Aymonier, P. Subra, L. Prat, C. Gourdon and E. Mignard, *Lab Chip*, 2011, **11**, 779-787.
18 M. T. Guo, A. Rotem, J. A. Heyman and D. A. Weitz, *Lab Chip*, 2012, **12**, 2146-2155.
19 Y. Zhu and Q. Fang, *Anal. Chem. Acta*, 2013, **787**, 24-35.
20 Q. Brosseau, J. Vrignon and J-C. Baret, *Soft Matter*, 2014, **10**, 3066-3076.
21 D. Lee, C. Fang, A. S. Ravan, G. G. Fuller, A. Q. Shen, *Lab Chip*, 2017, **17**, 717-726.
22 J. T. Cabral and S. D. Hudson, *Lab Chip*, 2006, **6**, 427-436.
23 B. J. Adzima and S. S. Velankar, *J. Micromech. Microeng.*, 2006, **16**, 1504-1510.
24 D. Ramirez-Gutierrez, C. Nieto-Draghi, N. Pannacci, L. V. Castro, F. Alvarez-Ramirez and B. Creton, *Langmuir*, 2015, **31**, 1400-1409
25 plug im ! software platform for data processing, IFPEN, 2018, www.plug-im.fr
26 N. Hardy, M. Moreaud, G. Denis, F. Augier, A. Nienow, C. Béal, F. Ben Chaabane, *J. Microsc.*, 2017, **266**, 126-140.
27 P.-Y. Gires, D. Barthes-Biesel, E. Leclerc, A.-V. Salsac, *J Mech Behav Biomed Mater*, 2016, **58**, 2.
28 F. P. Bretherton, *J. Fluid Mech.*, 1961, **10**, 166.
29 G. I. Taylor, *Proc. R. Soc. A*, 1934, **146**, 501-523.
30 K. Zografos, F. Pimenta, M. A. Alves, M. S. N. Oliveira, *Biomicrofluidics*, 2016, **10**, 43508.
31 D. Barthes-Biesel and A. Acrivos, *J. Fluid Mech*., 1973, **61**, 1-22.
32 J. M. Rallison, *Annu. Rev. Fluid Mech.,* 1984, **16**, 45-66.
33 Tregouët C., Salez T., Monteux C., Reyssat M., *Phys. Rev. Fluids*, 2018, **3**, 053603.
34 C. N. Baroud, F. Gallaire, R. Dangla, *Lab Chip*, 2010, **10**, 2032–2045.
35 S-Y. Park and P. Dimitrakopoulos, *Soft Matter*, 2013, **9**, 8844-8855.
36 M. Moiré, Y. Peysson, B. Herzhaft, N. Pannacci, F. Gallaire, L. Augello, C. Dalmazzone and A. Colin, *Langmuir*, 2017, **33**, 2531-2540.
37 K. Wang, L. Zhang, W. Zhang, G. Luo, *Langmuir,* 2016, **32**, 3174−3185.
38 N. J. Alvarez, D. R. Vogus, L. M. Walker, S. L. Anna, *J. Colloid Interface Sci.,* 2012, **372**, 183−191.
39 T. Glawdel and C. L. Ren, *Phys. Rev. E*, 2012, **86**, 026308.
40 F. Sarrazin, K. Loubière, L. Prat, C. Gourdon, T. Bonometti, J. Magnaudet, *AIChE J.*, 2006, **52**, 4061.
41 S.D. Hudson, *Rheol. Acta*, 2010, **49**, 237.
42 A. Nadim, H. A. Stone, *Stud. Appl. Math.*, 1991, **85**, 53.
43 A. D. Stroock, S. K. W. Dertinger, A. Ajdari, I. Mezic, H. A. Stone, G. M. Whitesides, *Science*, 2002, **295**, 647.
44 T. J. Kwak, Y. G. Nam, M. A. Najera, S. W. Lee, J. R. Strickler, W.-J. Chang, *PloS one*, 2016, **11**, e0166068.